University of Texas Rio Grande Valley
ScholarWorks @ UTRGV

Theses and Dissertations

12-2019

Photocatalytic Degradation of Simazine under Visible Light Using Zinc Oxide/Molybdenum Disulfide Heterostructures

Alexandria Castillo
The University of Texas Rio Grande Valley

Follow this and additional works at: https://scholarworks.utrgv.edu/etd

Part of the Chemistry Commons

Recommended Citation

Castillo, Alexandria, "Photocatalytic Degradation of Simazine under Visible Light Using Zinc Oxide/Molybdenum Disulfide Heterostructures" (2019). *Theses and Dissertations*. 430.
https://scholarworks.utrgv.edu/etd/430

This Thesis is brought to you for free and open access by ScholarWorks @ UTRGV. It has been accepted for inclusion in Theses and Dissertations by an authorized administrator of ScholarWorks @ UTRGV. For more information, please contact justin.white@utrgv.edu, william.flores01@utrgv.edu.

PHOTOCATALYTIC DEGRADATION OF SIMAZIME UNDER VISIBLE LIGHT USING ZINC OXIDE/MOLYBDENUM DISULFIDE HETEROSTRUCTURES

A Thesis

by

ALEXANDRIA CASTILLO

Submitted to the Graduate College of
The University of Texas Rio Grande Valley
In partial fulfillment of the requirements for the degree of

MASTER OF SCIENCE

December 2019

Major Subject: Chemistry

PHOTOCATALYTIC DEGRADATION OF SIMAZINE UNDER VISIBLE LIGHT USING ZINC OXIDE/MOLYBDENUM DISULFIDE HETEROSTRUCTURES

A Thesis
by
ALEXANDRIA CASTILLO

COMMITTEE MEMBERS

Dr. Jason G. Parsons
Chair of Committee

Dr. Evangelia Kotsikorou
Committee Member

Dr. Arnulfo Mar
Committee Member

Dr. Erik Plata
Committee Member

December 2019

Copyright 2019 Alexandria Castillo

All Rights Reserved

ABSTRACT

Castillo, Alexandria, Photocatalytic Degradation of Simazine Under Visible Light Using Zinc Oxide/Molybdenum Disulfide Heterostructures. Master of Science (MS), December, 2019, 56 pp, 13 figures, 5 tables, 46 references, 38 titles.

The photocatalytic degradation of simazine under visible light by using ZnO/MoS_2 heterostructures was investigated. Reaction parameters studied to optimize simazine degradation included pH, loading mass of the photocatalyst, and percentage of MoS_2 in the heterostructure. pH 2 was the optimal environment for the degradation reaction of all catalysts. A loading mass of 20 mg for each of the ZnO/MoS_2 photocatalysts was determined to be the most effective for in the degradation process. The degradation reactions were observed to follow 2^{nd} order kinetics for all photocatalysts at all temperatures. Band gap studies confirmed a lower energy than that of pure ZnO for all synthesized photocatalysts.

DEDICATION

Without the love and support of my parents, David and Maria Castillo, the completion of my master studies would not have been possible. In addition, I would like to thank Javier Cantu for the love and patience that motivated me to continue pushing forward and finish this degree. There are not enough words to express my love and gratitude for you all.

ACKNOWLEDGMENTS

I would like to thank Dr. J. G. Parsons, chair of my thesis committee, for the time and effort he invested in me. Without his mentorship the completion of my master’s degree would not have been possible. Thanks to his encouragement to continue my education I would not have had the courage to continue with doctoral studies. To my thesis committee members: thank you for the support and guidance that helped me accomplish this part of my educational career.

To my lab mates Kenneth Flores, Daniel Ramirez, Joe Lara, Rick Luna, Alexis Echeverria, John Paul Valle, and Valeria Velasquez: thank you for your friendship and support, without you, the countless hours spent in the research lab would have not been so worthwhile.

TABLE OF CONTENTS

Page

ABSTRACT……………………………………………………………………………….. iii

DEDICATION……………………………………………………………………………... iv

ACKNOWLEDGMENTS………………………………………………………………….. v

TABLE OF CONTENTS…………………………………………………………………... vi

LIST OF TABLES……………………………………………………………………….. viii

LIST OF FIGURES……………………………………………………………………….... x

CHAPTER I. BACKGROUND……………………………………………………………. 1

Simazine Mode of Action & Regulated Use…………………………………………... 1

Endocrine Disruption & Toxicity……………………………………………………... 2

Degradation……………………………………………………………………………. 3

CHAPTER II. INTRODUCTION………………………………………………………….. 5

Photocatalysis…………………………...…………………………………………….. 5

Generation of Reactive Oxygen Species………………………………………………. 6

Modification of Photocatalysts………………………………..………………………. 7

ZnO……………………………………………………………………………………. 8

MoS_2……………………………………………………………………………….. 10

ZnO/MoS_2…………………………………………………………………………. 11

CHAPTER III. MATERIALS AND METHODS………………………………………… 13

Synthesis of ZnO/MoS_2……………………………………………………………. 13

Synthesis of MoS_2…………………………………………………………………. 13

XRD Characterization……………………………………………………………….. 14

Band Gap Determination…………………………………………………………….. 14

HPLC Analysis……………………………………………………………………… 14

Degradation Studies……………………………………………………………….. 14

pH Study……………………………………………………………………………... 15

Loading Study………………………………………………………………………... 15

Kinetics Study………………………………………………………………………... 15

Concentration Variance……..……………………………………………………….. 15

CHAPTER IV. RESULTS AND DISCUSSION…………………………………….... 17

X-Ray Diffraction.…………………………………………………………………… 17

pH Study……………………………………………………………………………... 22

Photocatalyst Loading Study………………………………………………………… 24

Degradation Kinetics………………………………………………………………… 25

Concentration Variance………………………………………………………………. 27

Band Gap Study……………………………………………………………………… 29

CHAPTER V. CONCLUSIONS….…………………………………………………. 30

REFERENCES……………………………………………………………………….. 33

BIOLOGICAL SKETCH…………………………………………………………….. 38

LIST OF TABLES

Page

Table 1: Lattice parameters for all synthesized photocatalyst………………………………….. 21

Table 2: Rate constants (10^{-4}) ($L*mg^{-1}*s^{-1}$) for degradation by Zn/MoS_2 (3, 6, 12, 6% n/c) at 20, 30, and 50°C……………………...…………………………………………………….. 26

Table 3: Instantaneous rates (10^{-3}) ($mg*L^{-1}*s^{-1}$) of degradation by Zn/MoS2 (3, 6, 12%) at 20°C with an initial simazine concentration of 15 ppm……………….…….……………......... 27

Table 4: Instantaneous rates (10^{-3}) ($mg*L^{-1}*s^{-1}$) of degradation for Zn/$MoS_{2\ (3,\ 6,\ 12\%)}$ at 20°C with an initial simazine concentration of 15 ppm…………..………………………………... 28

Table 5: Calculated band gap for ZnO/MoS_2 photocatalysts…………………………………… 29

LIST OF FIGURES

Page

Figure 1: Degradation pathways of simazine (a) to 2-hydroxy-4,6-bis(ethylamino)-s-triazine (b), 2-chloro-4-amino-6-(ethylamino)-s-triazine (c) 2-chloro-4,6-diamino-s-triazine (d)………………………………………………………………………………………… 4

Figure 2: Reactive oxygen species generated from photooxidation and photoreduction………... 7

Figure 3: Three crystal structures of ZnO: rocksalt (a), zinc blende (b), and wurtite (c)………... 9

Figure 4: Top and lateral view of the crystal structures of 1T, 2H, and 3R polytypes…………. 11

Figure 5: Proposed mechanism of organic pollutant degradation by ZnO/MoS_2 composites under visible light……………………………………………………………………………… 12

Figure 6: Diffraction pattern and fittings for ZnO/$MoS_{2\ 3\%\ wt}$………………………………….. 17

Figure 7: Diffraction pattern and fittings for ZnO/$MoS_{2\ 6\%\ wt}$…………………. ……………… 18

Figure 8: Diffraction pattern and fittings for ZnO/$MoS_{2\ 6\%\ n/c\ wt}$ ………………………………. 19

Figure 9: Diffraction pattern and fittings for ZnO/$MoS_{2\ 12\%\ wt}$ ………………………………… 20

Figure 10: pH of simazine and corresponding degradation by ZnO/MoS_2 (3%, 6%, 12% wt MoS_2), pure MoS_2, and ZnO/$MoS_{2\ 6\%\ wt\ n/c}$..…………………………………….............. 22

Figure 11: Percentage of simazine removed per milligram of ZnO/MoS_2 (3%, 6%, and 12% wt MoS_2)……………………………………………………………………………………… 24

Figure 12: Kinetic plot for ZnO/$MoS_{2\ (3,\ 6,\ 6\ n/c,\ 12\%)}$ at 20 °C…………………..………………... 25

Figure 13: Percent simazine degradation at 5, 15, 25 ppm for ZnO/MoS_2 (3, 6, 12% wt)……... 28

CHAPTER I

BACKGROUND

Simazine Mode of Action & Regulated Use

Simazine is a symmetrical chloro-s-triazine herbicide. It is primarily utilized for the control of broad leaf weeds and annual grasses in agricultural, non-agricultural settings, as an algicide in fish farm ponds, algicide in water towers, and as an algicide aquariums.[1] Simazine is effectively distributed throughout the weed, however it can primarily be found in the leaves.[2] In annual grasses and broad leaf weeds, simazine inhibits the photosynthetic electron transport process in the leaves. Photosynthesis occurs in the chloroplasts of plants; the chloroplasts inner membranes are organized into sacs called thylakoids. In the thylakoids, after a photon of light excites the photosystem, the main electron acceptor plastiquinone is reduced and starts a chain reaction of enzyme catalyzed events that generate ATP and NADPH. When simazine is present, it binds to plastiquinone, preventing the photosynthetic electron transport process, stopping CO_2 fixation and the production of ATP and NADPH.[3] The weed plants can no longer survive due to their inability to reoxidize plastiquinone thus making simazine an effective herbicide.

Pesticides and herbicides are frequently employed in agriculture to increase crop yield. However, over application has led to the leaching of these organic pollutants into water supplies used as sources for drinking water. Concerns with the detection of increased concentrations of simazine in water sources around the world have led to regulations regarding its usage. Simazine is one of the most commonly detected herbicides in ground and surface water in the United

States.[3-5] This is due to the fact that it is widely used for weed control in North and South America in various application such as vineyards, orchards, and forestry,[7-9.] Europe banned the use of simazine in the early 2000s.[10] In the US in the Midwest, 90% of the 2 million pounds applied is to corn crops; in California, 90% of the 1 million pounds applied is to almonds, grapes, oranges, and walnuts; in Florida, 100% of the 1 million pounds applied is to citrus, including grapefruit and oranges.[11] The maximum containment level in drinking water has been set at 4.0 parts per billion. The regulation of simazine has come from the determination that it is an endocrine disrupting chemical.

Endocrine Disruption & Toxicity

Regulations have been enacted to protect the population from the potential risks of acute and chronic exposure to simazine. Endocrine disrupting chemicals, as the name suggests, interfere with the body's endocrine system. When an endocrine disruptor is present in the body it can interfere with the synthesis, transportation, binding, and/or action of natural hormones[12], therefore affecting the reproductive and developmental health of the organism. Triazine herbicides have been shown to directly affect the reproductive health of amphibians and rodents.[13,14] A case study was performed on California farmers, predominately Hispanic, to help identify the risks of prostate cancer from exposure to pesticides. The case study concluded that the risk of developing prostate cancer increased with the increased exposure to simazine.[15]

The US EPA has categorized simazine in Toxicology Category III for dermal and inhalation routes of exposure and Toxicology Category IV for the oral exposure route. The median lethal dose for oral exposure is greater than 5g/kg, greater than 2g/kg for dermal exposure, and 1.71 mg/L for inhalation. In spite of the regulated use, simazine is still being found in many drinking water sources.

Degradation

Finding way to successfully eliminate the presence of toxic herbicides in our drinking water has become a very important environmental issue. The degradation of simazine by abiotic and biotic processes is dependent on physicochemical properties such as solubility and sorption capacity, which contribute to its movement into water systems. Simazine is slightly soluble in water (5.0 mg/L at 20°C) and weakly adsorbs to clays, mineral rich and sandy soils.[1] Therefore, these surfaces cannot retain simazine leading to the chemical leaching into water. On the other hand, simazine has a greater sorption capacity to soils containing organic matter.[1] The presence of organic matter in the soil limits the leaching of simazine.

Simazine has a variety of degradation pathways. Figure 1 depicts the major abiotic and biotic degradation pathways. Hydrolysis involves the production of 2-hydroxy-4,6-bis(ethylamino)-s-triazine (3b) from simazine (3a). Biotic oxidation and photolysis of simazine yields 2-chloro-4-amino-6-(ethylamino)-s-triazine (3c) and 2-chloro-4,6-diamino-s-triazine (3d). Abiotic degradation through photolysis is potentially a promising route for removing simazine. Photocatalytic degradation of s-triazines under ultra-violet radiation has been thoroughly studied.[16] However, UV radiation only accounts for about 4% of natural sunlight. Under natural conditions simazine can persist in the environment for approximately 8 months.[1] Biotic degradation involves the presence of bacterial or fungal strains capable of dechlorinating the ring structure and hydrolyzing the ring, as well as dealkylating the amine side chains. Numerous microbial strains capable of degrading s-triazines have been identified[17]; however, degradation by biotic means is relatively slow.[1] Even though simazine is degradable naturally, its persistence in the soil and eventual leaching into our drinking water calls for the development of better methods to remove it from our drinking water.

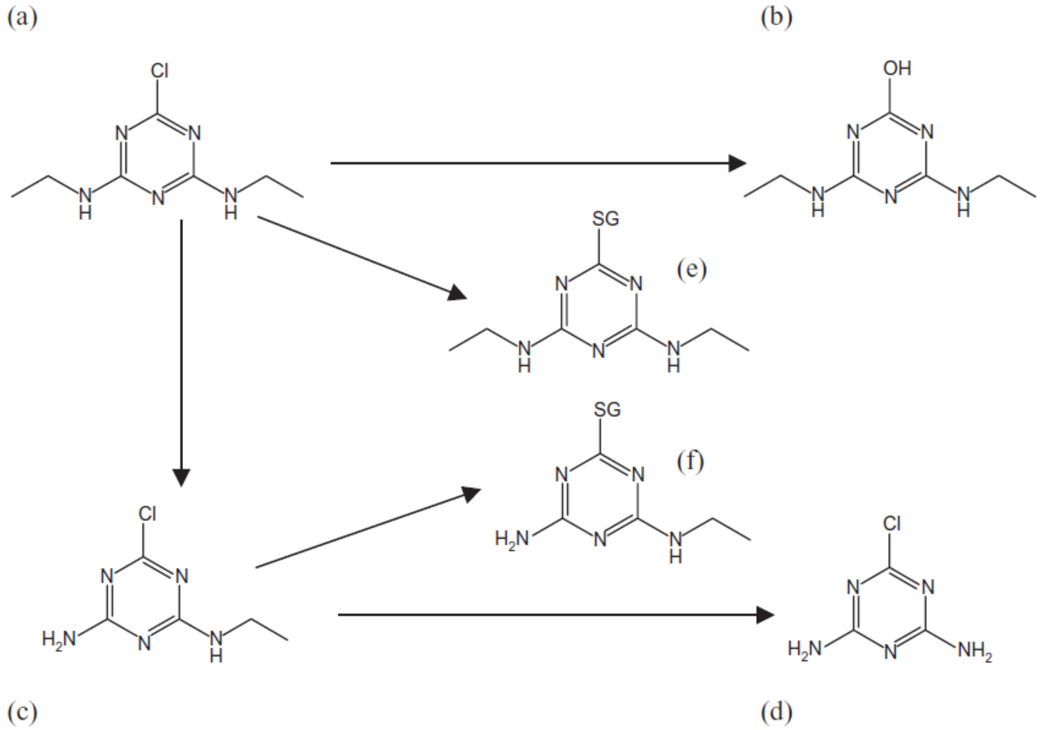
(a)
(b)
(c)
(d)
(e)
(f)
Cl
OH
SG
N
H
H_2N
NH_2

Figure 1: Degradation pathways of simazine (a) to 2-hydroxy-4,6-bis(ethylamino)-s-triazine (b), 2-chloro-4-amino-6-(ethylamino)-s-triazine (c) 2-chloro-4,6-diamino-s-triazine (d)[1]

CHAPTER II

INTRODUCTION

Photocatalysis

Photocatalysis is a process in which photons interact with a semiconducting material generating an electron-hole pair upon excitation of an electron. The excited is electron from the lowest unoccupied molecular orbital, conductive band, to the highest occupied molecular orbital, valence band in the semiconducting material. The semiconducting material is considered a photocatalyst because it changes the rate of a chemical reaction when irradiated. The degradation of organic pollutants[18,19], and hydrogen production by water splitting[20], are just a few examples of the reactions of photocatalysts.

Photocatalysts are generally also known as semiconductors. For a material to be classified as a semiconductor it must have a band gap between 1.5 to 3.0 eV. Band gap refers to the energy difference between the conductive and valence band and is related to the energy required to excite an electron from the former to the latter. Materials can be divided into three categories according to their band gap which includes: conductors, semiconductors, and insulators. When a photocatalyst is exposed to a wavelength of light that is equal to or greater than the band gap energy, an electron promotion occurs and formation of an electron and electron hole pair creates two locations for photo-reduction and photo-oxidation processes to occur. Recombination of the electron with the electron hole can occur, however, the properties of semiconductors are designed to avoid the recombination process. In solutions, species responsible for the potential redox processes are considered to be reactive oxygen species (ROS). Photocatalytic reactions involving advanced oxidative processes are dependent on the ROS generated by the photocatalyst.[21]

Generation of Reactive Oxygen Species

Photocatalytic reactions performed in an aqueous and aerobic environment will generate ROS simultaneously from the water and oxygen present. Figure 2 illustrates the generation of the four major ROS present in photocatalysis: superoxide anion radical ($\bullet O_2^-$), hydrogen peroxide (H_2O_2), singlet oxygen (^1O), and hydroxyl radical ($\bullet OH$). Photo-reduction occurs near the conductive band where the photoexcited electrons are promoted. Sequential photo-reduction of molecular oxygen produces a superoxide radical (1), which can be further reduced to a peroxide ion, O_2^{2-} (2). From the protonation of each two molecular orbitals hydrogen peroxide is generated (3). The hydrogen peroxide can be further reduced to also give the hydroxide radical after the dissociation of its O-O bond.

$$O_2 + e^- \rightarrow \bullet O_2^- \ (1)$$

$$\bullet O_2^- + e^- \rightarrow O_2^{2-} \ (2)$$

$$O_2^{2-} + 2H^+ \rightarrow H_2O_2 \ (3)$$

$$H_2O_2 \rightarrow \bullet OH + \bullet OH \ (4)$$

Photo-oxidation processes occur at the conductive band of the photocatalyst, the site of the electron holes. After the autoionization of water in which H_2O deprotonates to yield hydroxide ions, OH^-, and H^+(4), the hydroxide ions are oxidized to hydroxyl radicals (5). The two-hole oxidation of water also yields hydrogen peroxide.

$$H_2O \rightarrow OH^- + H^+ \ (4)$$

$$OH^- \rightarrow e^- + \bullet OH \ (5)$$

The generation of the four major ROS will dictate the efficiency of the semiconductor employed for the photocatalyic degradation of organic pollutants. Modification of photocatalysts is needed sometimes to increase ROS generation and improve the overall efficiency of advanced oxidation reactions.

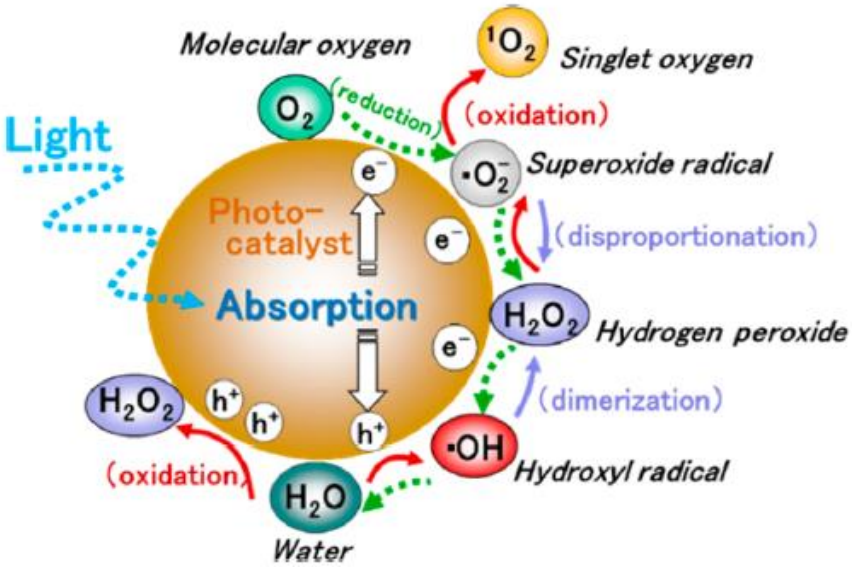

Molecular oxygen
$^1O_2$
Singlet oxygen
O_2
(reduction)
(oxidation)
Light
$\cdot O_2^-$
Superoxide radical
e^-
Photo-catalyst
e^-
(disproportionation)
Absorption
H_2O_2
Hydrogen peroxide
e^-
H_2O_2
h^+
h^+
(dimerization)
h^+
$\cdot OH$
Hydroxyl radical
(oxidation)
H_2O
Water

Figure 2: Reactive oxygen species generated from photo-oxidation and photo-reduction[21]

Modification of Photocatalysts

Metal oxides are the largest group of materials utilized as photocatalysts. However, most of the transition metal oxides have a large band gap, which limits their photoexcitation to the UV region. Although an obvious disadvantage, the generally high band gap energy of transition metal oxides can be modified a number of ways. These modifications are a way of tuning the electronic structure, therefore affecting the charge carrier mobility of the reactive oxygen species. In addition, modification helps prevent recombination of the excited electron with the hole in the valance band.

Semiconductors can be doped with metals or nonmetals, or a mixture of both. Doping with a metal, nonmetal, or a combination of both can reduce the band gap and shift the responsiveness of the material to the visible light region. Metal dopants such as Co, Cr, and Zn for example can create a new band below the conductive band of the semiconductor.[22] Doping with non-metals such as carbon, nitrogen, and sulphur can decrease the bandgap of wide band gap semiconductors into the visible light region by creating a new band above the valence band of the semiconductor.[22,23] The presence of a metal or nonmetal dopant can help avoid the recombination of the excite electron with the electron hole therefore increasing the photocatalytic activity of the material.

Semiconductors with variable band gaps can be combined to form photocatalytic composites. A photocatalyst with a large band gap is normally paired to one with a narrower band gap, which electrons from the conductive band of the narrower band gap semiconductor transfer to the conductive band of the larger band gap semiconductor.[24,25] Extensive research has been performed on composites containing ZnO due to its wide tunable band gap.[26]

Sensitization is another method of modifying photocatalysts. Complexes with chromophores that absorb visible light such as dyes are attached to the semiconductor. When irradiated with visible light, the sensitizer will transfer their electrons to the conductive band of the photocatalyst. The method of sensitization is not as reliable for the degradation of organic pollutants. The sensitizer may be degraded along with the other organic compounds, as well extra steps in the synthesis of the photocatalyst need to be taken to prevent the degradation of the sensitizer.[27,28]

ZnO

Zinc oxide is among the most studied metal oxides in photocatalysis alongside titanium dioxide. This is due to its large excitation binding of 60 mV and wide band gap of 3.37 eV. ZnO has been used for the photocatalytic degradation of dyes, and other persistent organic pollutants.[29,30] ZnO has three crystal structures: cubic rock-salt, cubic zinc-blende and hexagonal wurtzite (Figure 3). Hexagonal wurtzite is the most abundant and thermodynamically stable of the three.

The wide band gap of ZnO limits photocatalyis to the UV region. Therefore, modifications such as those mentioned earlier are necessary in order to enhance the photocatalytic activity of ZnO into the visible region. Ultimately, the goal of photocatalysis is to synthesis a material that will work affectively under natural sunlight. Zinc oxide continues to be a favorable candidate because its band gap is tunable. Doping with n-type metal ions, which act as electron donors, creates a level above the valance band of ZnO; while doping with p-type metal ions, which act as electron acceptors, creates a level below the conductive band of ZnO.[31] Another popular modification of ZnO is the formation of nanocomposites with another semiconducting material such as TiO_2, SnO, graphene, CdS, and CuO.[26] While all nanocomposites exhibit different photocatalytic activity, the literature shows that ZnO can be enhanced and function in the visible range.

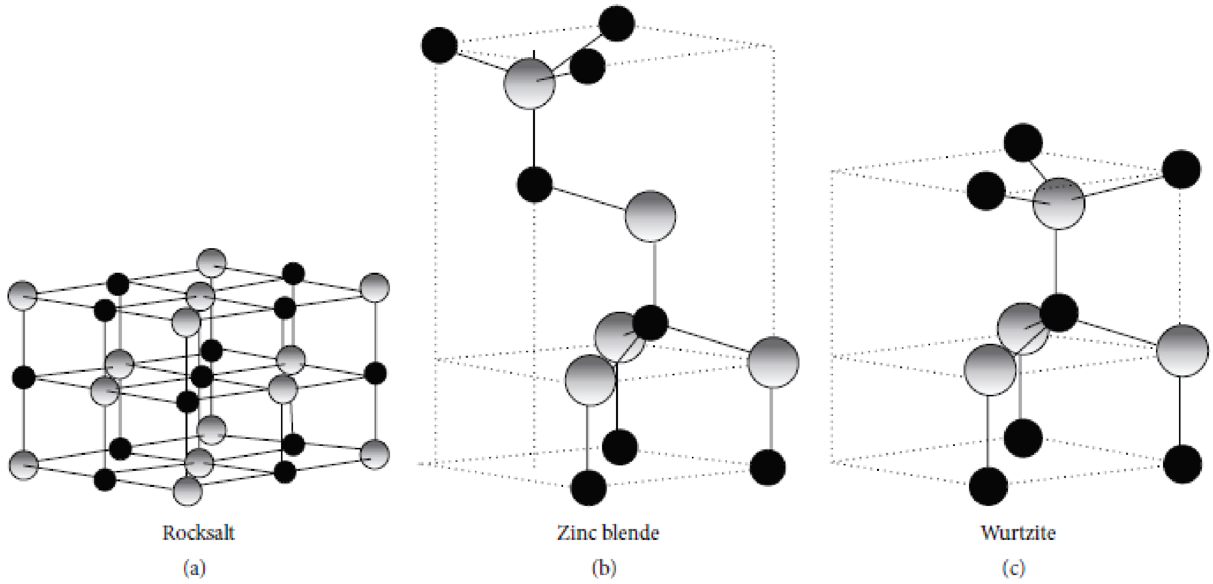

Figure 3: Three crystal structures of ZnO: rocksalt (a), zinc blende (b), and wurtzite (c)[26]

MoS_2

Molybdenum disulfide is a transition metal dichalcogenide with a number of industrial application including hydrogen desulfurization and dry lubricants.[32] MoS_2 is a nontoxic and naturally abundant material. The structure of bulk MoS_2 is comprised of S-Mo-S stacked layers held together by weak van-der-Waals interactions. There are four known polytypes of MoS_2: 1H, 1T, 2H, and 3R.[33] Three of the four polymorphs are shown in Figure 4. The number represents the stacking order of each layer while the letter denotes the crystallographic structure. In the 1H and 2H polytypes the central molybdenum atom is coordinated to six sulfur atoms creating a hexagonal structure. There are two repeating layers in 2H-MoS_2 and only one in 1H-$MoS_{2.}$ It has been determined that 2H-MoS_2 is the most stable of the four polytypes. In the 1T polytype, the coordination of the sulfur atoms to the central molybdenum atom creates a trigonal structure. In the 3R-MoS_2 polytype three layers from a rhombohedral structure.

The many layers of bulk MoS_2 can be separated by means of chemical and mechanical exfoliation[34], therefore changing the electronic properties of MoS_2 as the number of layers decreases. By controlling the morphology and reducing the amount of layers the photocatalytic performance of this material can be improved. MoS_2 based photocatalysts have recently become of interest because of this discovery. MoS_2 has helped facilitate the photocatalytic generation of hydrogen from water splitting.[35,36] The 1.2 eV indirect band gap of bulk molybdenum disulfide is too small to induce photocatalytic reactions. However, as the number of layers in the structure decrease, the band gap increases to 1.9 eV for single layer MoS_2 making it a feasible semiconductor for photocatalysis.[37,38]

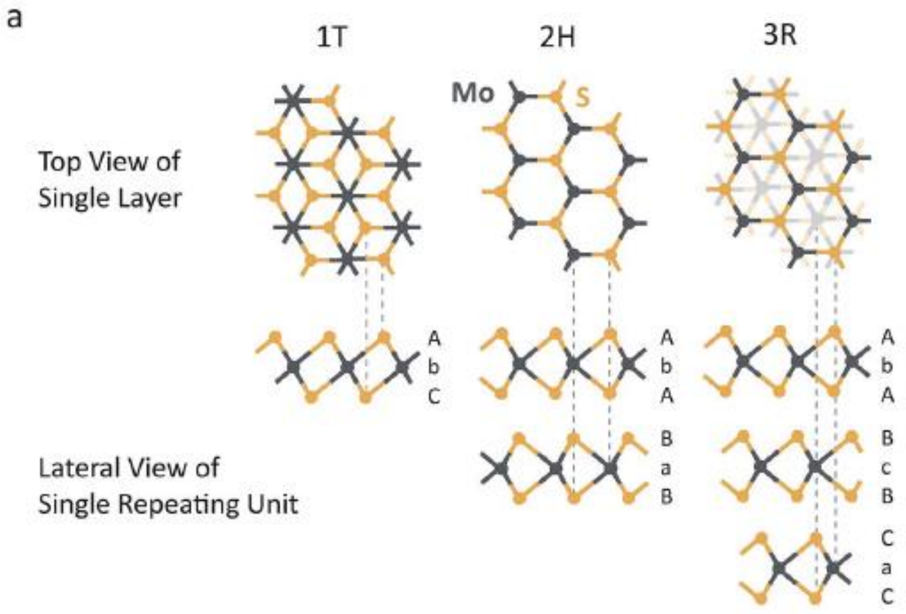

Figure 4: Top and lateral view of the crystal structures of 1T, 2H, and 3R polytypes[29]

ZnO/MoS_2

A ZnO/MoS_2 composite shows great promise as a photocatalytic material. As previously mentioned, ZnO despite having a high electron carrier mobility is limited by its high recombination rate of electron-hole pairs, its wide band gap which restricts its absorption ability to the UV region.[39] The direct band gap of small layer MoS_2 and strong absorption in the visible region can enhance the photocatalytic activity of ZnO and help minimize the fast recombination of ZnO, while the high charge carrier mobility of ZnO compensates for the low charge carrier mobility of MoS_2.[40] ZnO/MoS_2 heterostructures have been proven to photocatalytically degrade organic dyes under visible light.[41,42] Figure 4 illustrates the mechanism for the photocatalytic degradation of organic compounds by ZnO/MoS_2 composites under visible light. Upon irradiation, electrons in the valence band of both ZnO and MoS_2 are excited. The electrons from the conductive band in the MoS_2 are transferred to the lower conductive band of ZnO. Exited holes are simultaneously transferred from the valence band of ZnO to the higher MoS_2 valence band. Photo-oxidation occurs at the valence band of MoS_2 while photo-reduction occurs at the conductive band of ZnO.

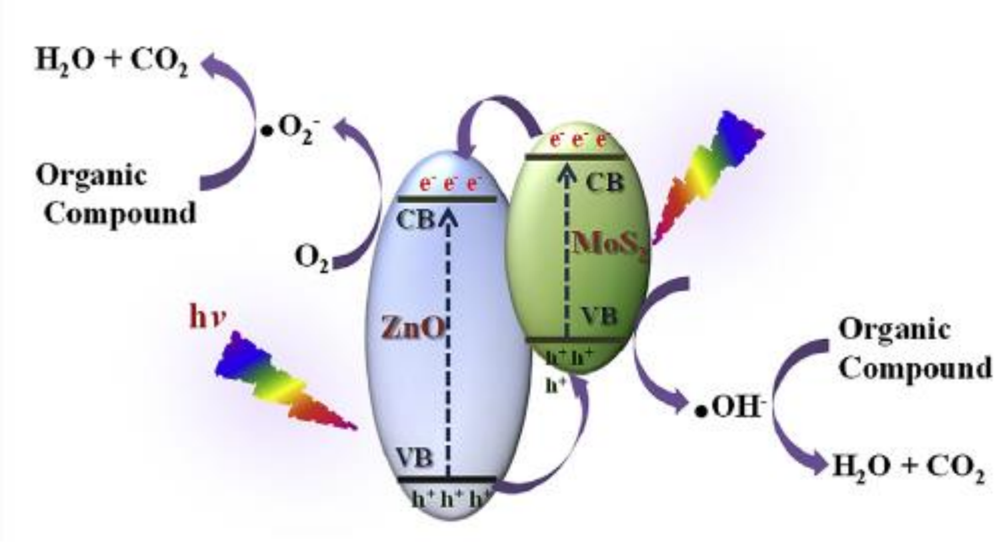
$H_2O + CO_2$
$\bullet O_2^-$
Organic Compound
O_2
hν
e⁻ e⁻ e⁻
CB
ZnO
VB
h⁺ h⁺ h⁺
e⁻ e⁻ e⁻
CB
MoS_2
VB
h⁺ h⁺
h⁺
$\bullet OH^-$
Organic Compound
$H_2O + CO_2$

Figure 5: Proposed mechanism of organic pollutant degradation by ZnO/MoS_2 composites under visible light[4]

CHAPTER III

MATERIALS AND METHODS

Synthesis of ZnO/MoS_2

Four zinc oxide/molybdenum disulfide heterostructures were prepared and tested for their photocatalytic efficiency. ZnO/MoS_2 was synthesized by adding 200 mg (6% wt) of commercial molybdenum disulfide to 10 mL of Millipore water and sonicated in a blank for 3 hours. 2.0 g of hexamethylenetriamine and zinc nitrate hexahydrate were added to two separate beakers containing 40 mL of Millipore water and stirred for 30 minutes. After 30 minutes, the two respective solutions were mixed and stirred for 1 hour. The sonicated MoS_2 solution was added to the hexamethylenetriamine and zinc nitrate hexahydrate mixture. The solution was then pH adjusted to ~11 with 1M and 5M NaOH solutions. The solution was added to a Teflon lined stainless steel autoclave and placed in an oven at 140°C for 2 hours. The resulting material once cooled to room temperature was filtered and washed with Millipore water, methanol, and acetone. Separate solutions of 100 mg (3%) and 400 mg (12% wt) of MoS_2 were also prepared. A fourth photocatalyst, ZnO/$MoS_{2\ (6\%\ wt\ n/c)}$ was prepared with 200 mg of noncommercial (n/c) MoS_2 synthesized in the laboratory.

Synthesis of MoS_2

To a 250 mL round bottom flask, 5 g of ammonium heptamolybdate tetrahydrate, 60 mL of ammonium sulfide, and 50 mL ammonium hydroxide were added. The mixture was refluxed at 70°C for 1 hour. The solution was cooled in an ice bath to crystallize, then filtrated and washed with cold isopropanol. The resulting crystals were placed into a porcelain crucible, and heated to 450°C for 1 hour inside a Thermolyne tube furnace under constant flow of H_2/Ar (10%/90%) mixture.

XRD Characterization

All photocatalysts were characterized using a Bruker D2 Phaser X-Ray Diffractometer equipped with a cobalt x-ray source that emits x-rays at 1.79Å, and a Fe filter. Samples were analyzed from a 2ϴ angle of 10-80°, a 0.05° step size, and counting time step of 2 seconds. The diffraction pattern fittings were performed with Fullprof software and crystallographic structures from the literature.[26,32]

Band Gap Determination

All photocatalysts were analyzed for band gap using a Perkin Elmer Lamda 950 UV-VIS-NIR Spectrophotometer. Measurements were recorded in %Reflectance from a range of 200-800 nm.

HPLC Analysis

The simazine samples from the degradation studies were analyzed using a Thermo ScientificUltimate 3000 High Performance Liquid Chromatograph (HPLC). The HPLC was equipped with a reverse phase C18 column and photodiode detector with UV-Vis lamps set to 220 and 225 nm. The mobile phase was comprised of 35/65 acetonitrile/acetate buffer (0.1M, pH 6) solution. 10 µL aliquots of each sample were injected into the column at a flow rate of 1 mL per minute, with a sample run time of 7 minutes.

Degradation Studies

Degradation studies were performed in a New Brunswick Scientific Innova 44 incubator under a 100W metal halide lamp. Degradation studies were performed for ZnO/$MoS_{2\ x}$ (x = 3%

wt, 6% wt, 12% wt) photocatalysts and MoS_2. Simazine samples were reacted with each photocatlyst in 10 mL beakers under the metal halide lamp for the desired amount of time and temperature under constant agitation. After each reaction, the samples were centrifuged for 5 minutes at 3500 rpm and the supernatants were decanted and analyzed. All reactions were performed using triplicate measurements for QA-QC and statistical purposes.

pH Study

All photocatalysts were tested over a pH range of 2 to 8. The reactions were performed using 25 ppm simazine solutions were pH adjusted. The pH adjustments were performed using either dilute HCl and or dilute NaOH solutions. 4 mL of pH adjusted simazine solution was added to 20 mg of photocatalyst and irradiated with visible light for 1 hour at 20°C.

Loading Study

The amount of photocatalytic material was varied from 10, 20, 40, and 80 mg to assess the optimal amount needed for simazine degradation. The reactions were performed at 20°C for 1 hour, with 4 ml aliquots of 25 ppm simazine at the optimal pH determined from the pH study.

Kinetics Study

To determine the degradation reaction kinetics 4 ml aliquots of 25 ppm simazine solutions at the optimal pH and photocatalyst loading mass were irradiated with visible light for 2 hours at 20, 30, and 50°C. As the photocatalytic reaction proceeded, 1.5 μL aliquots of each sample were taken for HPLC analysis.

Concentration Variance

The concentration of simazine was varied at 5 ppm, 15 ppm, and 25 pm. All three photocatalysts were reacted with 4 ml of simazine at each concentration, optimal pH and loading mass for 1 hour under visible light at 20°C. For 15 and 25 ppm samples, 1.5μL aliquots were extracted every 15 minutes, centrifuged for 5 minutes at 3500 rpm, and analyzed. The 5 ppm samples, 1.5µL aliquots were taken every 5 minutes and analyzed. From the data, the Gibbs free energy, enthalpy, entropy and activation energy of the degradation reaction was calculated.

CHAPTER IV

RESULTS AND DISCUSSION

X-Ray Diffraction

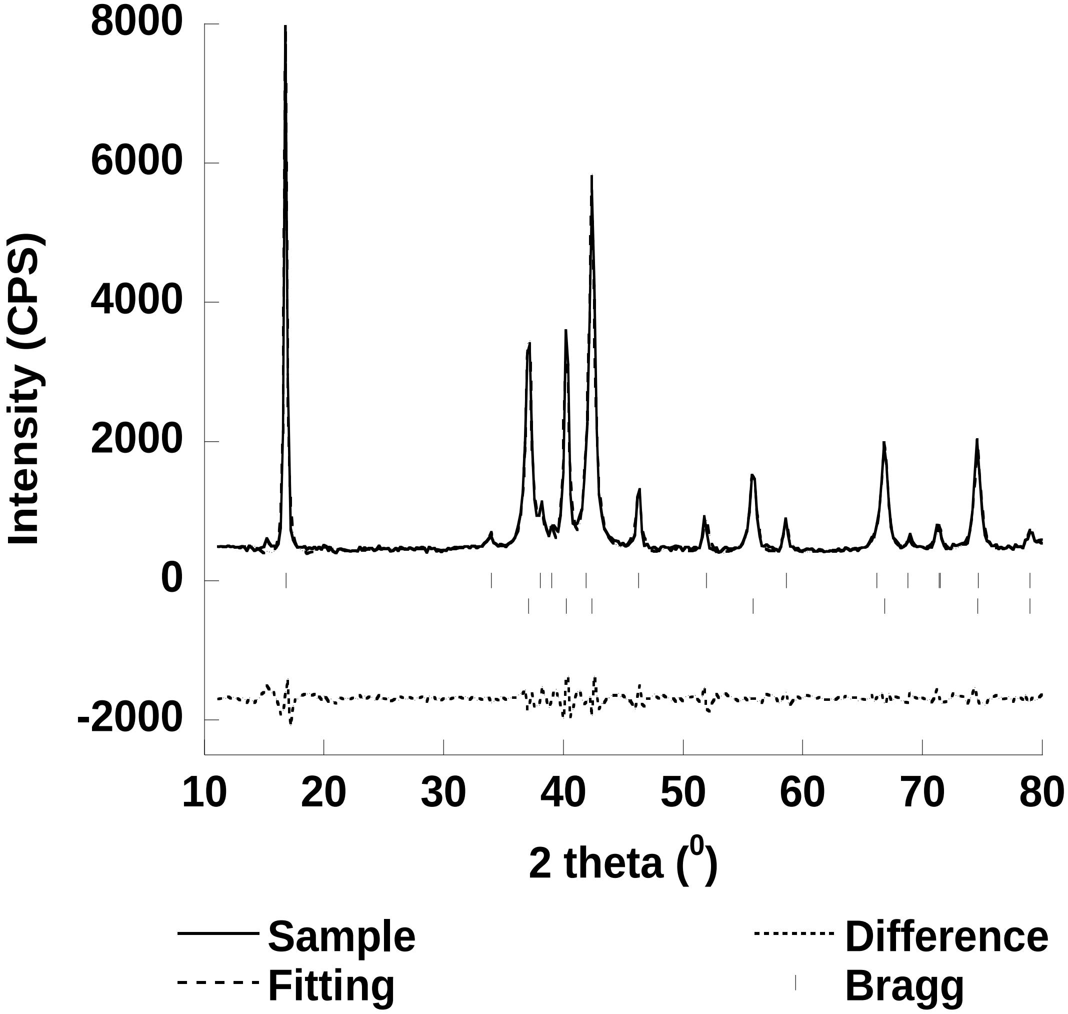

Figure 6: Diffraction pattern and fittings for ZnO/$MoS_{2\ 3\%\ wt}$

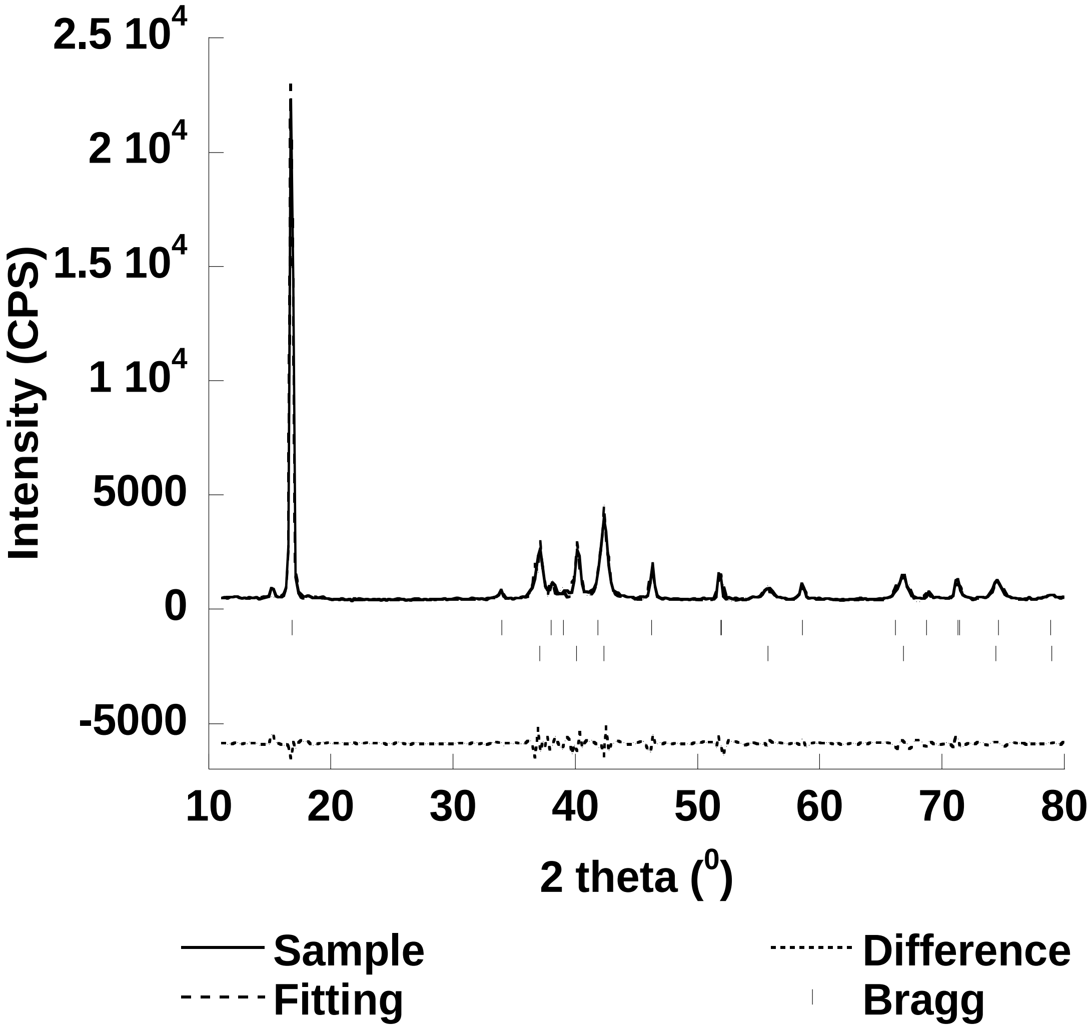

Figure 7: Diffraction pattern and fittings for ZnO/$MoS_{2\ 6\%\ wt}$

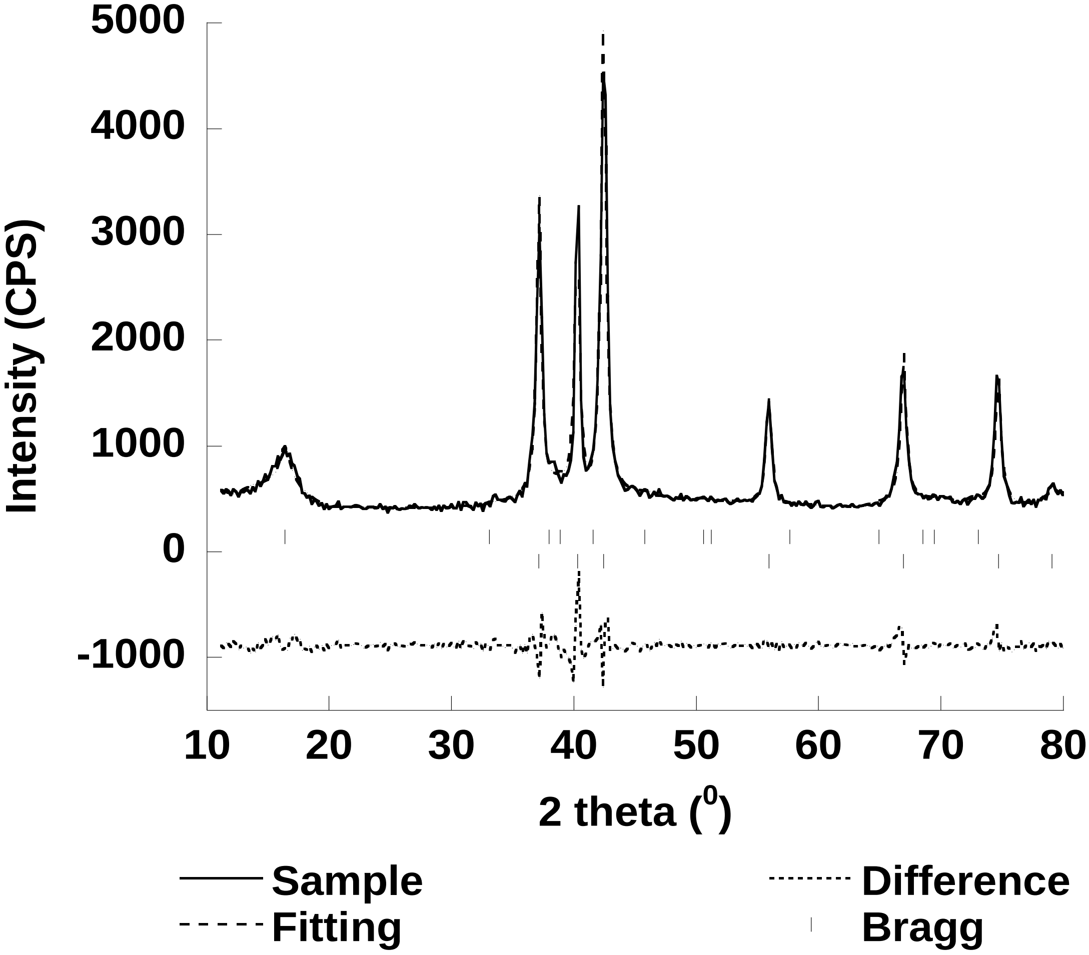

Figure 8: Diffraction pattern and fittings for ZnO/$MoS_{2\ 6\%\ n/c\ wt}$

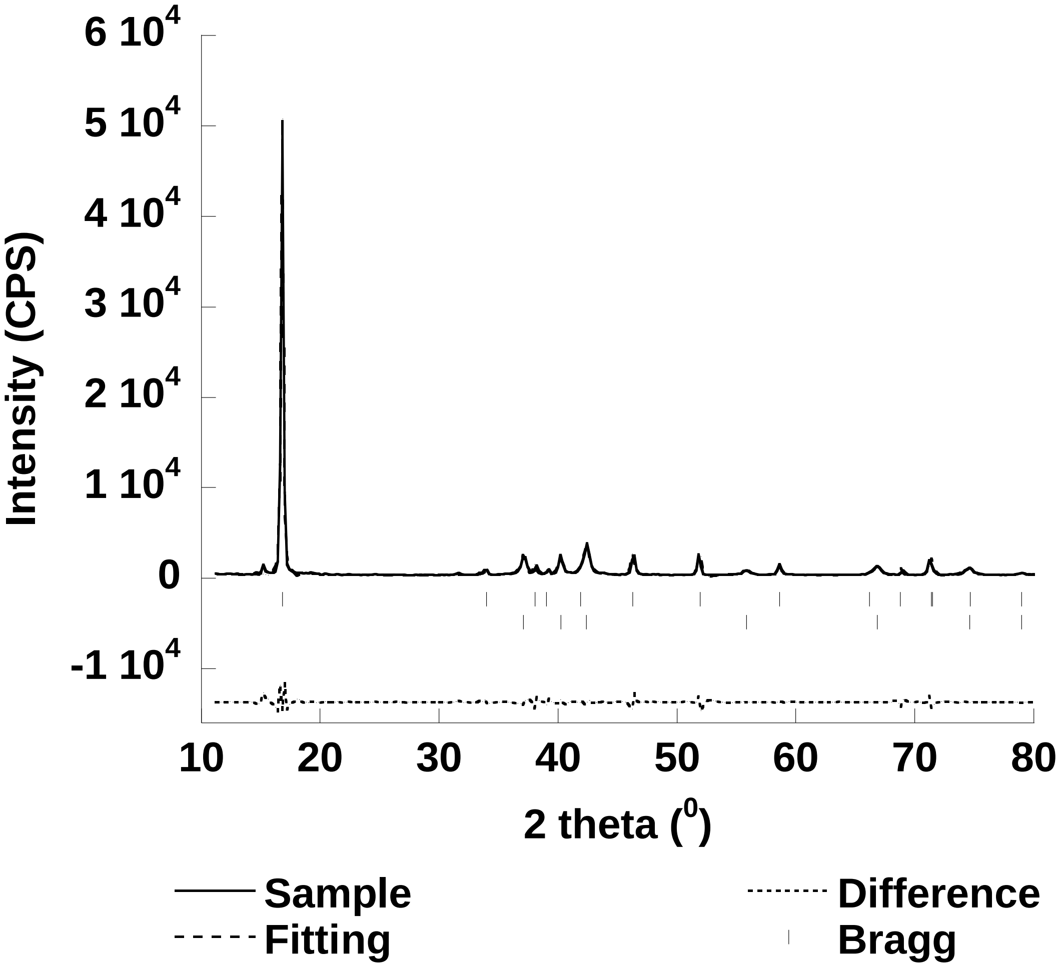

Figure 9: Diffraction pattern and fittings for $ZnO/MoS_{2\ 12\%\ wt}$

Sample	**Lattice**	**a(Å)**	**b(Å)**	**c(Å)**	**α, β, γ**	**X^2**
3%	P63/mmc P63/mc	3.1689 3.2505	3.1689 3.2505	12.2574 5.2042	90,90,120 90,90,120	6.15
6%	P63/mmc P63/mc	3.1714 3.2500	3.1714 3.2500	12.2567 5.2209	90,90,120 90,90,120	7.12
6% n/c	P63/mmc P63/mc	3.1787 3.2464	3.1787 3.2464	12.2572 5.2001	90,90,120 90,90,120	3.264
12%	P63/mmc P63/mc	3.1689 3.2505	3.1689 3.2505	12.257 5.2042	90,90,120 90,90,120	10.22

Table 1: Lattice parameters for all synthesized photocatalyst

Fitted diffraction patterns for all synthesized photocatalysts are shown in Figures 6-9. The solid line indicates the diffraction pattern for the sample while the larger dashed line indicates the diffraction fitting. The smaller dashed line indicates the difference between the diffraction pattern and fitting; and the vertical markings indicate the Bragg planes.

All ZnO/MoS_2 photocatalysts displayed a hexagonal crystal structure for the ZnO and MoS_2 phases present in the material, and lattice parameters consistent with literature values.[26,32] A summarization of these parameters are shown in Table 1. ZnO conformed to the hexagonal wurtzite crystal structure with space group, P63/mc. The average values for the lattice parameters of each photocatalyst were a = b = 3.25 Å, and c = 5.20 Å. MoS_2 conformed to the 2H-MoS_2 polytype with space group, P63/mmc. The average lattice parameters of each photocatalyst were a = b = 3.17 Å, and c = 12.26 Å. The angles α, β, and γ were 90, 90, and 120, respectively.

The first major peak seen in all diffraction patterns corresponds to the (002) plane in MoS_2. The intensity of the diffraction peak increased as the mass percent of MoS_2 increased in the sample. There is a significant difference in the intensity of the (002) peak between ZnO/$MoS_{2\ 6\%}$ and ZnO/$MoS_{2\ 6\%\ n/c}$. The decrease in intensity for the sample synthesized with noncommercial MoS_2 is related to the number of layers of MoS_2 present, not the mass percent. There is less stacking in noncommercial MoS_2. The intensity of five major peaks at 37°, 40°, 42°, 55°, and 66° (2Ɵ) from the ZnO crystal structure remained constant for all photocatalysts, as the concentration of ZnO remained constant. The (100) plane is represented by the diffraction peak at 37°. The (002) plane showed reflectance at 40°, and the (101) plane showed reflectance at 42°. At 55° and 66°, the (102) and (110) planes showed reflectance, respectively.

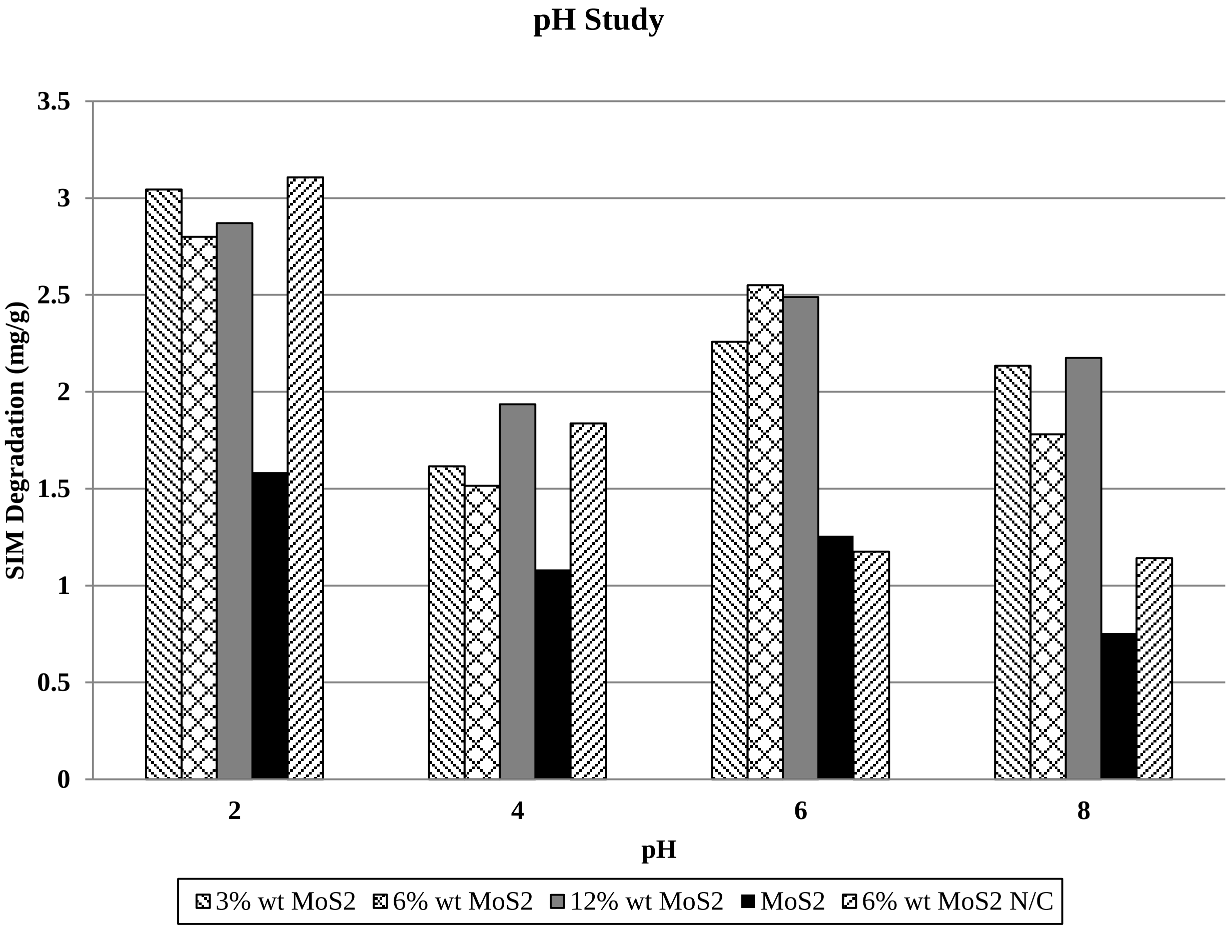

Figure 10: pH of simazine and corresponding degradation by ZnO/MoS_2 (3%, 6%, 12% wt), pure MoS_2, and $ZnO/MoS_{2\ 6\%\ wt\ n/c}$

The degradation of simazine over a 1 hour period and pH range of 2-8 was recorded in milligrams of simazine per gram of photocatalyst. The photocatalytic efficiency of ZnO/MoS_2

(3%, 6%, 6% n/c, and 12% wt MoS_2) and pure MoS_2 is displayed in Figure 5. At pH 2 the greatest amount of simazine degradation was observed. For all materials expect $ZnO/MoS_{2\ 6\%\ wt\ n/c}$, simazine degradation decreased from pH 2 to 4, increased from pH 4 to 6, then decreased again from pH 6 to 8. At pH 2, the simazine degradation was 3.044 mg/g for $ZnO/MoS_{2\ 3\%\ wt}$, 2.800 mg/g for $ZnO/MoS_{2\ 6\%\ wt}$, 2.871 mg/g for $ZnO/MoS_{2\ 12\%\ wt}$, 1.585 mg/g for pure commercial MoS_2, and 3.106 mg/g for $ZnO/MoS_{2\ 6\%\ wt\ n/c.}$ At pH 4 the least amount of simazine degradation was 1.616 mg/g, 1.515 mg/g, and 1.936 mg/g respectively for ZnO/MoS_2 (3%, 6%, 12% wt). A decrease in simazine degradation from pH 2 to pH 8 occurred for $ZnO/MoS_{2\ 6\%\ wt\ n/c}$. When comparing the $ZnO/MoS_{2\ 6\%\ wt}$ synthesized by commercial and non-commercial MoS_2, the mg/g of simazine degraded was greater with the ZnO/MoS_2 synthesized with non-commercial MoS_2. The amount degraded by the n/c photocatalyst is slightly greater than $ZnO/MoS_{2\ 3\%\ wt}$.

Introducing small amounts of MoS_2 to the ZnO structure has been shown to enhance the photocatalytic activity of ZnO.[31, 39, 41] However, excess amounts of MoS_2 can potentially hinder degradation by obstructing the light absorption efficiency of the ZnO material.[39] Higher amounts of MoS_2 do not result in greater simazine degradation, which is further evident when comparing the pH study data for the 3 wt% and 12 wt%. There was higher simazine degradation was observed for the 3 wt% catalyst. Although simazine degradation with 12 wt% was slightly higher than for the 6 wt%, this can be explained by the possible the adsorption of simazine to the MoS_2. Photodegradation by MoS_2 alone resulted in less than 30% simazine removal.

The photocatalytic efficiency of the material can be dependent on the concentration of simazine in the solution. According to Ward *et al.*, the solubility of simazine decreases from $5.81(10^{-4}\ M)$ at pH 1 to $0.25(10^{-4}\ M)$ at pH 10.[43] Furthermore, the solubility of simazine is based on the 2-substituent and the alkyl groups located at the 4- and 6- positions. The trend in solubility is similar to the trend in simazine degradation as pH increases. For reactions such as photocatalytic degradation involving the surface of semiconductors, pH plays a vital role in the surface charge properties of the semiconductor, which can affect photoredox processes.[44] For example, semiconducting materials generally are negatively charged will experience repulsion from negatively charged simazine in alkaline conditions.[45] In addition, H_2O_2 an important reactive oxygen species, is not stable in alkaline conditions and will not be able to perform carry out photo-oxidation.

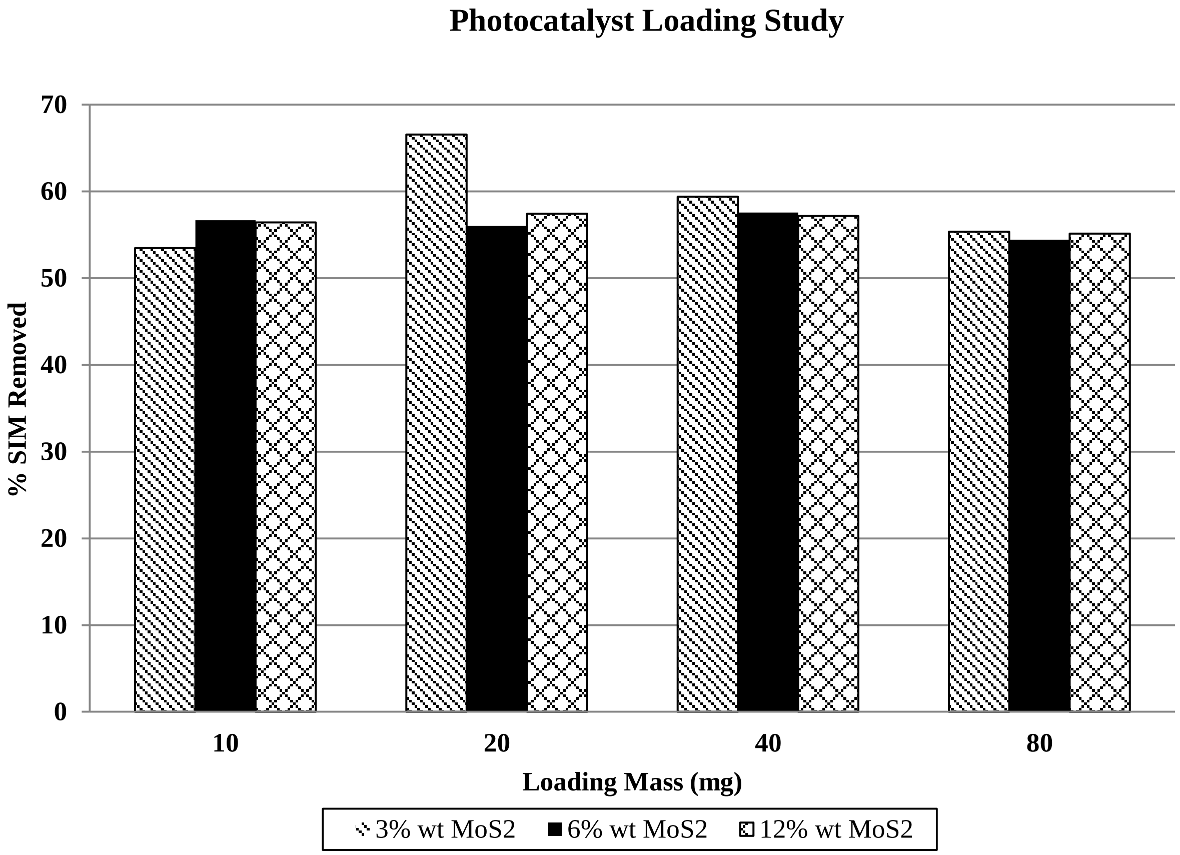

Figure 11: Percentage of simazine removed per milligram of ZnO/MoS_2 (3%, 6%, and 12% wt MoS_2)

The amount of photocatalyst present in the degradation reaction was varied from 10 to 80 milligrams for ZnO/MoS_2 (3%, 6%, and 12% wt MoS_2) at the optimal pH. The percentage of simazine removed by each photocatalyst was observed to range from 50 to 70 percent as shown in Figure 7. For ZnO/MoS$_{2\ 3\%\ wt}$ and ZnO/MoS$_{2\ 12\%\ wt}$, 20 mg of catalyst yielded 66.55% and 57.43% simazine degradation, respectively, an increase in removal compared to the 10 mg photocatalyst sample. There was approximately a 13% difference in the percent degradation between 10 mg and 20 mg of ZnO/MoS$_{2\ 3\%\ wt}$, and approximately 1% for ZnO/MoS$_{2\ 12\%\ wt}$. With both photocatalysts, the percent degradation was observed to slightly decrease at 40 mg and 80 mg. While 40 mg of ZnO/MoS$_{2\ 6\%\ wt}$ removed 57.57% of simazine in the reaction, 10 mg removed 56.68%, and 20 mg removed 56.01%. The largest difference occurred between 40 mg and 80 mg, where 80 mg of ZnO/MoS$_{2\ (6\%\ wt)}$ degraded 54.42%. Due to only slight differences in percent simazine degraded, 20 mg of photocatalyst were utilized for the following studies.

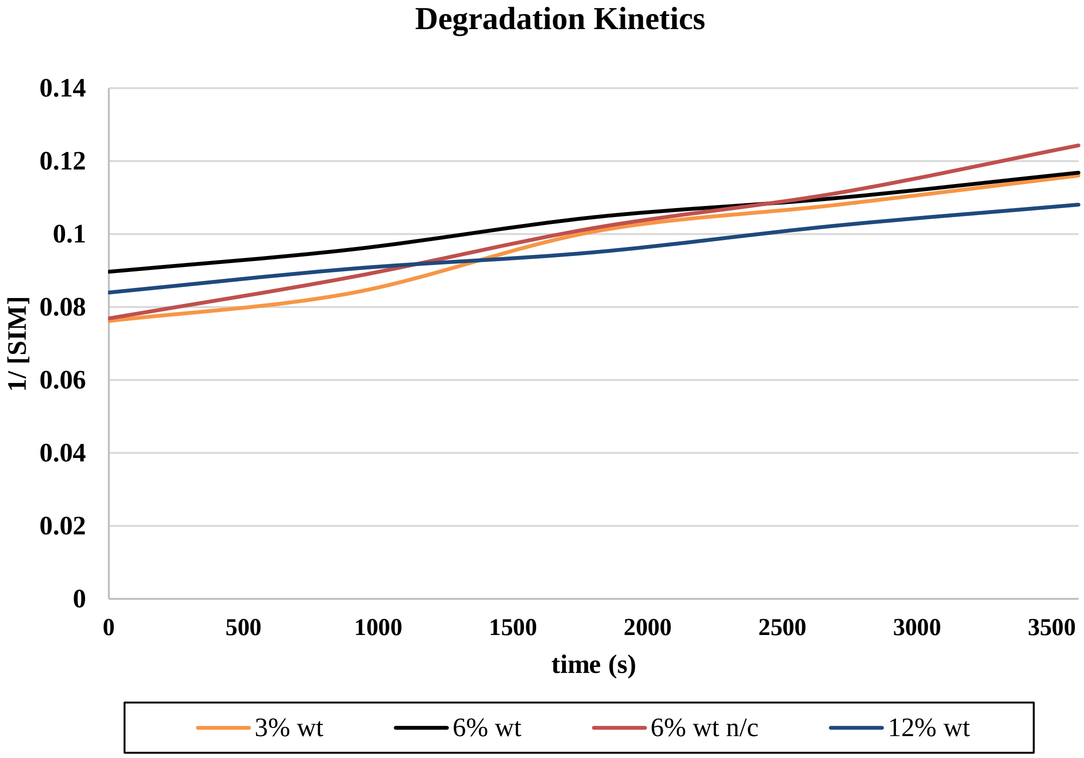

Figure12: Kinetic plot for ZnO/MoS$_{2\ (3,\ 6,\ 6\ n/c,\ 12\%)}$ at 20 °C

The degradation kinetics for a 1-hour reaction period at 20 °C by different ZnO/MoS_2 photocatalysts was determined by plotting the inverse of the concentration of simazine remaining as a function of time. The results are shown in Figure 8. The linear relationship between $\frac{1}{[SIM]}$ versus time indicated the degradation reaction occurred through 2nd order kinetics. The degradation at 30 and 50°C yielded similar results for all the photocatalysts studied. The slope of the 2nd order kinetics plot is equal to the rate constant for the reaction. Table 1 summarizes the determined rate constants and are expressed as $L*mg^{-1}*sec^{-1}$. For ZnO/MoS_2 (3, 6%) the highest rate of degradation was observed at 50°C. At 30°C the highest rate of degradation was observed for ZnO/MoS_2 (12%). When comparing the ZnO/MoS_2 (6%) synthesized by commercial and non-commercial MoS_2 the rate of degradation increased with the non-commercial MoS_2. When the temperature of the degradation reaction increased from 20 to 50°C the instantaneous rate, expressed as $mg*L^{-1}*sec^{-1}$, increased for the 3, 6, and 12% photocatalysts.

	20 °C	**30 °C**	**50 °C**
ZnO/$MoS_{2\ 3\%}$	6.93	6.27	7.61
ZnO/$MoS_{2\ 6\%}$	4.56	5.65	8.93
ZnO/$MoS_{2\ 12\%}$	4.00	7.45	6.12
ZnO/$MoS_{2\ 6\%\ n/c}$	6.69		

Table 2: Rate constants (10^{-4}) ($L*mg^{-1}*s^{-1}$) for degradation by Zn/$MoS_{2\ (3,\ 6,\ 12,\ 6\%\ n/c)}$ at 20, 30, & 50°C

	20 °C	**30 °C**	**50 °C**
ZnO/MoS$_{2\ 3\%}$	1.23	1.32	1.59
ZnO/MoS$_{2\ 6\%}$	0.697	1.07	1.75
ZnO/MoS$_{2\ 12\%}$	0.665	1.28	1.21
ZnO/MoS$_{2\ 6\%\ n/c}$	1.02		

Table 3: Instantaneous rates (10^{-3}) (mg*L^{-1}*s^{-1}) of degradation by Zn/MoS$_{2\ (3,\ 6,\ 12,\ 6\%\ n/c)}$ at 20, 30, & 50°C

Concentration Variance

To examine the effects of simazine concentration on the rate of degradation, the concentration was varied from 5 to 25 ppm at 20°C. The relationship between initial simazine concentration and simazine degradation is shown in Figure 9. As the concentration of simazine decreased from 25 ppm to 15 ppm, the percentage of simazine degraded decreased from 60.3 to 48.4% for ZnO/MoS$_{2\ 12\%\ wt}$, 64.1 to 51.0% for ZnO/MoS$_{2\ 6\%\ wt}$, and 59.8 to 50.9% for ZnO/MoS$_{2\ 3\%\ wt}$. However, with the initial concentration of simazine was 5 ppm, there was 0% degradation for ZnO/MoS$_{2\ (3,\ 12\%\ wt)}$, and only 3% degradation for ZnO/MoS$_{2\ 6\%\ wt.}$ The concentration of simazine greatly affects the efficiency of photocatalytic degradation. However, when comparing the instantaneous rates of degradation at 20°C when there was 25 ppm of simazine versus 15 ppm of simazine present, the rates for the degradation of 15 ppm were greater, as seen in Table 4.

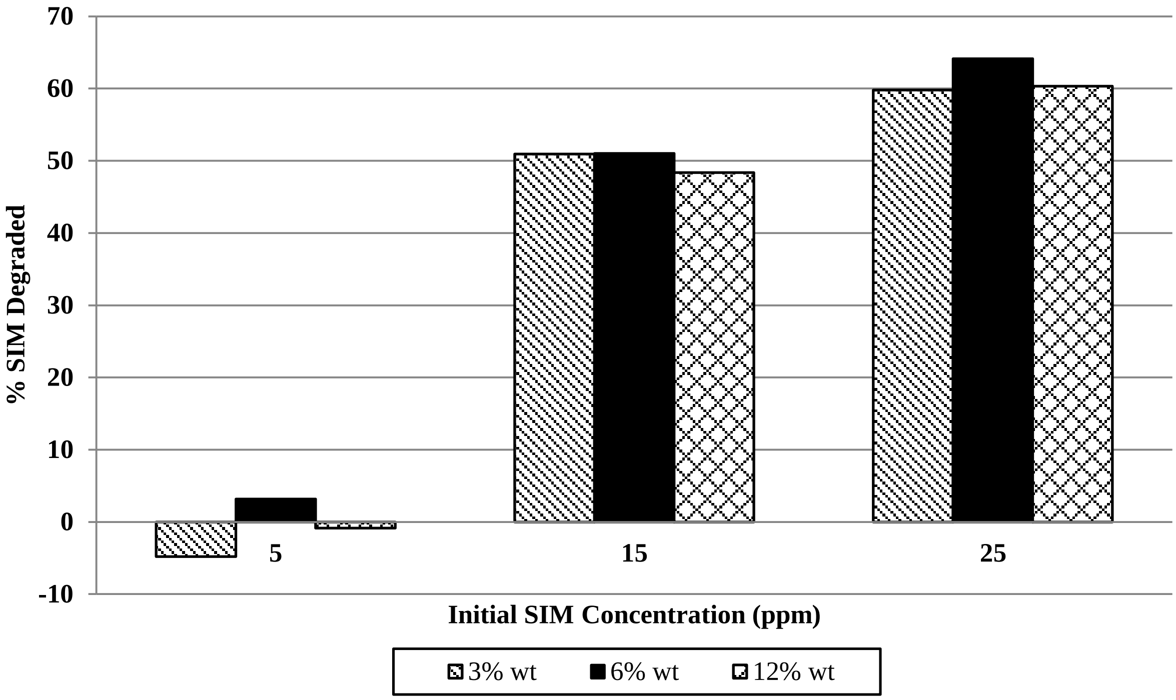

Figure 13: Percent simazine degradation at 5, 15, 25 ppm for ZnO/$MoS_{2\ (3,\ 6,\ 12\%\ wt)}$

Photocatalyst	**Instantaneous Rate**
ZnO/$MoS_{2\ 3\%}$	1.71
ZnO/$MoS_{2\ 6\%}$	0.811
ZnO/$MoS_{2\ 12\%}$	1.28

Table 4: Instantaneous rates (10^{-3}) (mg*L^{-1}*s^{-1}) of degradation by Zn/$MoS_{2\ (3,\ 6,\ 12\%)}$ at 20°C with an initial simazine concentration of 15 ppm

Band Gap Study

Photocatalyst	Band Gap (eV)
ZnO	3.37
ZnO/$MoS_{2\ 3\%}$	3.17
ZnO/$MoS_{2\ 6\%}$	3.22
ZnO/$MoS_{2\ 6\%\ n/c}$	3.23
ZnO/$MoS_{2\ 12\%}$	3.25

Table 5: Calculated band gap for ZnO/MoS_2 photocatalysts

Band gap values were calculated by the Kubelka-Munk fitting from % Reflectance data. The Kubelka-Munk fitting method is based on the following equation:

$$F(R) = \frac{(1-R)^2}{(2R)}$$

where R is equal to the reflectance, $(1\text{-R})^2$ is equal to the extinction coefficient, and (2R) is equal to the scattering factor.[46] By plotting F(R) as a function of energy (eV), the band gap can be extrapolated from the graph. When comparing the band gap for pure ZnO and the ZnO/MoS_2 heterostructures, there was a narrowing in valence and conductive band in all the ZnO/MoS_2 materials. By reducing the electrical potential of the material, the wavelength of radiation needed to initiate a photocatalytic process is closer to the visible light region. Wei *et al* reported similar band gap values when comparing the band gap of ZnO/MoS_2 quantum dots with that of pure ZnO.[41]

CHAPTER V

CONCLUSIONS

The photocatalytic activity of four ZnO/MoS_2 heterostructures was investigated. The photocatalysts varied in the percent by mass of MoS_2 present in the structure which ranged from 3 to 12%. X-ray diffraction and UV-Vis spectrophotometry were used to characterize the photocatalysts. The photocatalysts were tested on the ability to photo-catalytically degrade a triazine herbicide, simazine, under visible light. Reaction conditions such as the pH of simazine solution and the loading mass were investigated to determine the optimal conditions for efficient degradation.

The pH was varied from 2 to 8, and it was determined that pH 2 was the optimal pH for simazine degradation for all photocatalysts during a one-hour cycle. At pH 2, the amount of photocatalyst was varied from 10 to 80 mg. A loading mass of 20 mg was chosen for $ZnO/MoS_{2\ (3,\ 6,\ 12\%)}$. With 20 mg of material 66.55%, 56.01%, and 57.43% of the simazine was degraded within one hour for 3, 6, and 12% wt respectively. The effects of altering the loading mass were more apparent with the 3% wt. A pH of 2 and loading mass of 20 mg was used for the kinetics and concentration variance studies.

With the reaction conditions optimized the rate of simazine degradation was investigated over a 2-hour period at three different temperatures (20,30, and 50°C). By graphically plotting the $\frac{1}{[SIM]}$ as a function of time it was evident that the degradation process proceeded through 2nd order kinetics. At 20°C the rates degradation was as follows, 3% wt ($6.93x10^{-4}$ $L*mg^{-1}*s^{-1}$), 6%

wt (4.56×10^{-4} L*mg^{-1}*s^{-1}), 6 % wt noncommercial MoS_2 (6.69×10^{-4} L*mg^{-1}*s^{-1}), and 12% wt (4.00×10^{-4} L*mg^{-1}*s^{-1}). As the temperature increased from 20 to 50°C the rate of degradation increased. When the initial concentration of simazine was decreased from 25ppm to 15 ppm the percent of simazine degraded decreased from 59.78 to 50.947% for $ZnO/MoS_{2\ 3\%}$, from 64.13 to 51.04% for $ZnO/MoS_{2\ 6\%}$, and from 60.32 to 48.37% $ZnO/MoS_{2\ 12\%}$.When the concentration of simazine was 5 ppm the percent simazine degradation decreased to 0% for $ZnO/MoS_{2\ 3\%}$ and $ZnO/MoS_{2\ 12\%}$. $ZnO/MoS_{2\ 6\%}$only 3% simazine degradation was observed.

In addition, the excess amounts of MoS_2 present in the heterostructure can hinder the photocatalytic efficiency of the material by interfering with light absorption by ZnO. For the heterostructures comprised of commercial MoS_2 the 3% wt performed better than the 6, and 12% wt. Although only one catalyst prepared with noncommercial MoS_2 was studied, the preliminary data suggests that by using noncommercial MoS_2, which contains fewer layers, the degradation can be further enhanced.

UV-Vis spectrophotometric characterization of the photocatalysts yielded calculated band gap values less than that of pure ZnO, and greater than that of pure MoS_2 for all materials. This leads to the conclusion that by introducing MoS_2 to the structure of ZnO, the material can effectively function as a photocatalyst in the visible region.

X-ray diffraction characterization of the synthesized photocatalysts confirmed the presence of ZnO and MoS_2 in the heterostructure. The intensity of the diffraction peaks characteristic of ZnO remained the same for all materials. There was an increase in the intensity of the (002) diffraction peak for MoS_2 as the weighted percent of MoS_2 increased in the sample. When comparing the 6% heterostructures synthesized with and without commercial $MoS_{2,}$ it was found that the intensity of MoS_2 was significantly lesser in the sample with the noncommercial

MoS_2. The lower intensity in the 002 plane is possibly due to the decreased layers of MoS_2 in the noncommercial sample.

REFERENCES

1. Gunasekara, A. S., Troiano, J., Goh, K.S., Tjeerdema, R.S. (2007). Chemistry and fate of simazine. *Reviews of Environmental Contamination and Toxicology*, 189, 1-23.

2. Wilson, P.C., Whitwell, T., Klaine, S.J. (1999). Phytotoxicity, uptake, and distribution of [^{14}C] simazine in canna hybrid ‘yellow king humbert’. *Environmental Toxicology and Chemistry*, 18(7), 1462-1468.

3. Anhrens, W. 1994. Herbicide Handbook of the Weed Science Society of America. WSSA, Champaign, IL, USA.

4. Barbash, J.E., Thelin, G.P., Kolphin, D.W., Gilliom, R.J. (2001). Major herbicides in ground water: results from the national water-quality assessment. *Journal of Environmental Quality*, 30(3), 831-845.

5. Wilson, P. C., Lu, H., Lin, Y. (2011). Norflurazon and simazine removal from surface water using constructed wetland. *Bulletin of Environmental Contamination and Toxicology*, 87, 426-430.

6. Scribner, E.A., Thurman, E.M., Goolsby, D.A., Meyer, M.T., Battaglin, W.A., Kolpin, D. W. (2005). Summary of significant results from studies of triazine herbicides and their degradation products in surface water, ground water, and precipitation in the Midwestern united states during the 1990s. U.S. Geographical Survey Scientific Investigations Report 2005-5094, 27

7. Suarez, F., Guzman, E., Munoz, J.F., Bachmann, J., Ortiz, C. Kogan, M. (2013). Simazine transport in undisturbed soils from a vineyard at the Casablanca valley, Chile. *Journal of Environmental Management*, 117, 32-41.

8. Chang, N.B., Srilakshmi, K.R., Parvathinathan, G. (2008).Comparison of models of simazine transport and fate in the subsurface environment in a citrus farm. *Journal of Environmental Management*, 86, 27-43.

9. Morgante, V., Flores, C., Fadic, X., Gonzalez, M., Hernandez, M., Balic, F.C., Seeger, M. (2012). Influence of microorganisms and leaching on simazine attenuation in an agricultural soil. *Journal of Environmental Management*, 95, S300-S305.

10. Morgante, V., Lopez, A.L., Flores, C., Gonzalez, M., Gonzalez, B., Vasquez, M., Mora, R.R., Seeger, M. (2010). Bioaugmentation with pseudomonas sp.strain MHP41 promotes simazine attenuation and bacterial community changes in agricultural soils. *Federation of European Microbiological Ecology*, 71, 114-126.

11. US EPA. Registration Eligibility Decision For Simazine. (2006)1-266.

12. Park, S., Kim, S., Jin, H., Lee, K., Bae, J. (2014). Impaired development of female mouse offspring maternally exposed to simazine. *Environmental Toxicology and Pharmacology*, 38, 845-851.

13. Bimbaum, L.S., Fenton, S.E. (2003). Cancer and developmental exposure to endocrine disruptors. *Environmental Health Perspectives*, 111(4), 389-394.

14. Hayes. T.B., Stuart, A. A, Mendoza, M., Collins, A., Noriega, N., Vonk, A., Johnston, G., Liu, R., Kpodzo, D. (2006). Characterization of atrazine-induced- gonadal malformations in African clawed frogs (xenopus laevis) and comparison with effects of an androgen antagonist (cyproterone aceate) and exogenous estrogen (17-estradiol): support for the demasculinization/feminization hypothesis. *Environmental Health Perspectives*, 114, 134-141.

15. Mills, P.K., Yang, R. (2003). Prostate cancer risk in California farm workers. *Journal of Occupational and Environmental Medicine*, 45(3), 249-258.

16. Munoz, M.J., Aguado, J., Revilla, A. (2011). Photocatalytic removal of s-triazines: evaluation of operational parameters. *Catalysis Today*, 161, 153-162.

17. Guo, Q., Wan, R., Xie, S. (2014). Simazine degradation in bioaugmented soil: urea impact and response of ammonia-oxidixing bacteria and other soil bacterial communities. *Environment Science and Pollution Research*, 21, 337-343.

18. Dong, H., Zeng, G., Tang, L., Fan, C., Zhnag, C., He, X., He, Y. (2015). An overview on limitations of TiO2-bases particles for photocatalytic degradation of organic pollutants and the corresponding countermeasures. *Water Research*, 79, 128-146.

19. Tian, J., Leng, Y., Cui, H., Liu, H. Hydrogenated TiO2 nanobelts as highly efficient photocatalytic organic dye degradation and hydrogen evolution photocatalyst. *Journal of Hazardous Materials*, 299, 165-173.

20. Teets, T.S., Nocera, D.G. (2011). Photocatalytic hydrogen production. *Chemistry Communications*, 47, 9268-9274.

21. Nosaka, Y., Nosaka, A. Y. (2017). Generation and detection of reactive oxygen species in photocatalysis. *Chemical Reviews*, 117, 11302-11336.

22. Ameta, R., Solanki, M.S., Benjamin, S., Ameta, S.C. “Chapter 6 Photocatalysis. Advanced oxidation processes for waste water treatment”. Emerging Green Chemical Treatment. 135-175.

23. Marschall, R., Wang, L. (2014). Non-metal doping of transition metal oxides for visible-light photocatalysis. *Catalysis Today*, 225, 111-135.

24. Wang, X., Lui, G., Chen, Z., Li, F., Wang, L., Lu, G.Q., Cheng, H.M. (2009). Enhances photocatalytic hydrogen evolution by prolonging the lifetime of carriers in ZnO/CdS heterostructures. *Chemical Communications*, 23, 3452-3454.

25. Wang, M., Wang, W., Zhang, L. Sun, S., Wang, L., Zhou, L. (2009). 3D Bi2WO6/TiO2 hierarchical heterostructure: controllable synthesis and enhanced visible, photocatalytic degradation performances. *The Journal of Physical Chemistry C*, 113(33), 14727-14731.

26. Johar, M.A., Afzal, R.A., Alazba, A. A., Manzoor, U. (2015). Photocatalysis and Bandgap Engineering Using ZnO Nanocomposites. *Advances in Materials Science and Engineering*, 2015, 1-22.

27. Qin, G., Sun, Z., Wu., Q., Lin, L., Liang, M., Xue, S. (2011). Dye-sensitized TiO2 film with bifunctionalized zones for photocatalytic degradation of 4-cholophenol. *Journal of Hazardous Materials*, 192, 599-604.

28. Chowdhury, P., Moreira, J., Gomaa, H., Ray, A.K. (2012). Visible-solar-light-driven photocatalytic degradation of phenol with dye-sensitized TiO2: parametric and kinetic study. *Industrial & Engineering Chemistry Research*, 51, 4523-4532.

29. Khataee, A.R., Zarei, M. (2011). Photoelectrocatalytic decolorization of diazo dye by zinc oxide nanophotocatalst and carbon nanotube cathode: determination of the degradation products. *Desalination*, 278, 117-125.

30. Tran, M.L., Fu, C., Juang, R. (2018). Removal of metronidazole by TiO2 and ZnO photocatalysis: a comprehensive comparison f process optimization and transformation products. *Environmental Science and Pollution Research*, 25, 28285-28295.

31. Tian, N., Li, Z., Xu, D., Li, Y., Peng, W. Zhang, G., Zhang, F., Fan, X. (2016). Utilization of MoS2 Nanosheets To Enhance the Photocatalytic Activity of ZnO for Aerobic Oxidation of Benzyl Halides under Visible Light. *Industrial & Engineering Chemistry Research*, 55(32), 8726-8732.

32. Song, I., Park, C., Choi, H. (2015). Synthesis and properties of molybdenum disulphide: from bulk to atomic layers. *Royel Society of Chemistry Advances*, 5, 7495-7514.

33. Li, Z., Meng, X., Zhnag, Z. (2018). Recent Development on MoS2-based photocatalysis: A review. *Journal of Photochemistry and Photobiology C: Photochemistry Reviews*, 35, 39-55.

34. Yuan, Y., Lu, H., Yu, Z., Zou, Z. (2015). Nobel-metal-free molybdenum disulfide cocatalyst for photocatalytic hydrogen production. *ChemSusChem*, 8(24), 4113-4127.

35. Karundasa, H., Montalvo, E., Sun., Y., Majda, M., Long, J., Chang, C. (2012). A molecular MoS2 edge site mimic for catalytic hydrogen generation. *Science*, 335.

36. Hinnemann, B., Moses, P., Bonde, J., Jorgensen, K., Nielsen, J., Horch, S., Chorjendorff, I., Norskov, J. (2005). Biomimetic hydrogen evolution: MoS2 nanoparticles as catalyst for hydrogen evolution. *Journal of American Chemical Society*, 127, 5308-5309.

37. Cheiwchanchamnangij, T., Lambrecht, W. (2012). Quasiparticle band structure calculation of monolayer, bilayer, and bulk MoS2. *Physical Review B*, 85, 205302.

38. Mak, K.F., Lee, C., Hone, J., Shan, J., Heinz, T. F. (2010). Atomically thin MoS2: a new direct-gap semiconductor. *Physical Review Letters*, 105, 136805.

39. Awasthi, G. W., Adhikari, S. P., Ko, S., Kim, H. J., Park, C. H., Kim, C. S. (2016). Facile synthesis of ZnO flowers modified graphene like MoS2 sheets for enhanced visible-light-driven photocatalytic activity and antibacterial properties. *Journal of Alloys and Compounds*, 682, 208-215.

40. Kumar, S., Maivizhikannan, V., Drews, J., Krishnan, V. (2019). Fabrication of nanoheterostructures of boron doped ZnO-MoS2 with enhanced photostability and photocatalytic activity for environmental applications. *Vacuum*, 163, 88-98.

41. Mei, W., Chen, C. S., Chen, X., Lui, X., Yang, Z., Ding, F., Chao, Z., Liu, T. (2018). Low-temperature construction of MoS2 quantum dots/ZnO spheres and their photocatalytic activity under natural sunlight. *Journal of Colloid and Interface Science*, 530, 714-724.

42. Kumar, S., Sharma, V., Bhattacharyya, K., Krishnan, V. (2016). Synergetic effect of MoS2-RGO doping to enhance the photocatalytic performance of ZnO nanoparticles. *New Journal of Chemistry*, 40, 5185-5197.

43. Ward, T. M., Weber, J. B. (1968). Aqueous solubility of alkylamino-s-triazine as a function of pH and molecular structure. *Journal of Agricultural and Food Chemistry*, 16(6), 959-961.

44. Fenoll, J., Hellin, P., Martinez, C.M., Flores, P., Navarro, S. (2012). Semiconductor-sensitized photodegradation of s-triazine and chloroacetanilide herbicides in leaching water using TiO_2 and ZnO as catalyst under natural sunlight. *Journal of Photochemistry and Photobiology A: Chemistry*, 238, 81-87.

45. Rao, Y., Chu, W. (2013). Visible light-induced photodegradation of simazine in aqueous TiO_2 suspension. *Industrial & Engineering and Chemistry* Research, 52, 13580-13586.

46. Lopez. R., Gomez, R. (2012). Band-gap energy estimation from diffuse reflectance measurements on sol-gel and commercial TiO_2: a comparative study. *Journal of Sol-Gel Science Technology*, 61, 1-7.

BIOGRAPHICAL SKETCH

Alexandria Castillo was born in 1996 in McAllen, Texas to Perfecto D. Castillo and Maria P. Castillo. She grew up in Alamo, Texas and attended PSJA Memorial Early College High School where she graduated in May of 2014. She attended South Texas College during high school and completed an Associate of Science in Biology in May of 2014. Alexandria attended the University of Texas at San Antonio from August 2014 to May 2017 and graduated Cum Laude with General Honors from the Honors College with a Bachelor of Science in Chemistry. In the Fall of 2017, she enrolled at the University of Texas Rio Grande Valley and began the working towards a Master of Science in Chemistry. At the University of Texas Rio Grande Valley Alexandria was employed as a Teaching Assistant, Research Assistant, and conducted research while completing the degree curriculum. Alexandria graduated with her Master of Science in Chemistry in December of 2019. Alexandria Castillo's permanent address is 701 Margret Street Alamo, Texas 78516. Her personal email address is alexandria.castillo01@gmail.com.